Crystal-structure effects in the Ce L_3-edge x-ray-absorption spectrum of CeO_2: Multiple-scattering resonances and many-body final states

A. V. Soldatov and T. S. Ivanchenko
Department of Solid State Physics, Rostov University, Sorge Street 5, Rostov-Don, 344104 Russia

S. Della Longa
Dipartimento di Medicina Sperimentale, Università dell'Aquila, Coppito, 67100 L'Aquila, Italy

A. Kotani and Y. Iwamoto
The Institute for Solid State Physics, University of Tokyo, Tokyo 106, Japan

A. Bianconi
Dipartimento di Fisica, Università di Roma, "La Sapienza," 00185 Roma, Italy
(Received 3 December 1993)

Here we report the interpretation of all spectral features of Ce L_3 x-ray-absorption near-edge (XANES) structure of CeO_2 over a 40 eV range. The local partial unoccupied density of states in the initial state and in the fully relaxed final state have been calculated by the full multiple-scattering approach. The wave function of the excited electron in the final states of the Ce L_3-edge XANES spectrum is found to be determined by the multiple-scattering processes in a large size cluster formed by at least 45 atoms. We predict, in good agreement with the experimental data, the crystal-field splitting of $5d$ states in the final state $\Delta_f = 4.0 \pm 0.2$ eV and its variation from the initial to the final state. The many-body final states for the $2p \rightarrow 5, \varepsilon d$ transition, arising from the configuration interaction due to mixing of Ce $4f$ and O $2p$ valence orbitals, have been calculated taking into account the crystal-field splitting of the $5, \varepsilon d$ states and they give a full explanation for the low-energy shoulder on the Ce L_3 x-ray-absorption spectrum white line that was the object of a long-standing discussion. The origin of the pre-edge peak at about 10 eV below the white line maximum is explained as due to transitions at the bottom of the conduction band.

I. INTRODUCTION

The Ce atom is in a crossover region between elements (higher-Z elements) that keep the atomiclike character of f orbitals in condensed matter that form localized states, and elements (lower-Z elements) that form delocalized states.[1] The electrons in CeO_2 are at the borderline between localized and bandlike behaviors. In fact, evidence of large mixing of metal f and oxygen $2p$ orbitals has been found from theoretical linear augmented plane wave (LAPW),[2] linear muffin-tin orbital (LMTO) band-structure,[3] and molecular-orbital calculations for CeO_8 cluster.[4] Starting from the pioneering work of Vainsthein, Blokhin, and Paderno,[5] high-energy spectroscopies [x-ray photoemission (XPS), x-ray-absorption near-edge structure (XANES),[3,6–14] and electron-energy-loss spectra (EELS) (Refs. 15 and 16)] of the insulating $4f$ compound CeO_2 have attracted considerable interest. After long discussion[11–13] it has been found that the mixed valency of insulating CeO_2 in the final state is due to the hybridization of Ce $4f$ and O $2p$ states in the initial state. The main peak of Ce $L_{2,3}$ XANES in CeO_2, which is due to the $2p \rightarrow 5, \varepsilon d$ transition, clearly shows many-body final-state effects.[7] In fact, L_3 XANES of transition metals, actinides, and lanthanides exhibit a single white line at the threshold which is due to a resonance in the $2p \rightarrow 5d$ cross section modified by local density of unoccupied states, resulting in the $5, \varepsilon d$ final state. Conversely, Ce L_3-edge XANES of CeO_2 exhibits a fine structure, including two main white lines. Previously,[9] Ce L_3 XANES data have been treated by a many-body calculation in the framework of the Anderson impurity model.[17–20] Two main peaks in Ce L_3 XANES of CeO_2 are shown to arise from many-body final-state effects due to the mixing of multielectron configurations.[9] However, band-structure effects are not included in this model. The low-energy shoulder of main line in Ce L_3 XANES of CeO_2 and the pre-edge peak are still an unsolved puzzle. They were not obtained numerically in previous calculations. Up to now, only qualitative interpretations have been proposed: (1) shakedown satellites;[8] (2) a result of the quadrupole transition (for prepeak);[3] and (3) results of the transitions to the depopulated, mixed Ce $5d$–O $2p$ states during the relaxation process (for the low-energy shoulder).[3]

There are two main approaches to the interpretation of the x-ray spectroscopic data: (i) in terms of many-body configuration theory for a core transition to localized electronic states, and (ii) in terms of the one-electron band structure of the crystal for a core transition to delocalized electronic states.[2,3] The presence of two white lines in CeO_2 L_3-edge XANES was interpreted[7] as a breakdown of the one-electron description of a core transition, because these two peaks correspond to different

many-body final-state configurations. Therefore, Ce L_3 XANES of ionic systems have been interpreted mostly in terms of atomic transitions including many-body final-state effects, where the role of some important solid-state effects was neglected. We propose that one needs to take the band-structure effect into account while treating Ce $5,\varepsilon d$ electronic states in CeO_2.

Ce L_3 XANES spectra probe the unoccupied density of states of 5, εd and s symmetries selected by the dipole selection rules. Considering only the Ce coordination shell, the unoccupied $5d$ orbitals are expected to be split by the ligand field of the eight oxygen atoms on the vertices of the cube in the first-neighbor shell in e_g and t_{2g} orbitals at lower and higher energies, respectively, separated by the crystal-field energy splitting $\Delta_i = -10D_q$.[21] Here we show that introducing Ce $5d$ state crystal-field splitting in the initial state into the Anderson impurity model results in the appearance of a low-energy shoulder in the calculated Ce L_3-edge XANES of CeO_2. We also show that the pre-edge peak in Ce L_3-edge XANES of CeO_2 is a result of the transition at the unoccupied states at the bottom of the CeO_2 conduction band.

II. MULTIPLE-SCATTERING CALCULATION

Here we have applied the multiple-scattering approach in real space to calculate Ce L_3 XANES of CeO_2. In spite of the relatively large number of K-edge XANES full multiple-scattering analyses in various materials (see for review, Refs. 22 and 23), only a few multiple-scattering calculations devoted to L_3 XANES (Refs. 24–28) have been carried out.

The algorithm for full multiple scattering method we used in this study was described earlier.[29] For the calculation we use a fluorite-type structure with a lattice constant equal to 5.411 Å.[30] The cluster of neighbor atoms around a central Ce is divided into shells, as reported in Table I. The muffin-tin radii and the muffin-tin constants that we obtained according to our procedure for muffin-tin potential construction[31] are reported in Table II (both for the unrelaxed potential, appropriate for the initial state, and for the fully relaxed potential, appropriate for the final state in the presence of the core hole). While constructing the crystal potential we use the muffin-tin approximation according to the Mattheiss prescription, with an exchange parameter equal to 1.0. Atomic charge densities were obtained with the help of the self-consistent Dirac-Slater method.

TABLE I. Structure of the five-shell cluster for CeO_2.

Coordination shell	Atom	Number of atoms in shell	Number of atoms in cluster	Sphere radii (Å)
1	O	8	9	2.343
2	Ce	12	21	3.828
3	O	24	45	4.487
4	Ce	6	51	5.411
5	O	24	75	5.896

TABLE II. The muffin-tin radii R_{mti} (Å) of the elements included in CeO_2 and the muffin-tin constants $-V_{0i}$ (eV).

Atoms	R_{mt} (Å)		$-V_{0i}$ (eV)	
	Unrelaxed	Relaxed	Unrelaxed	Relaxed
Ce (central)	1.3998	1.4720	−21.358	−25.920
Ce (other)	1.3998	1.4720	−21.358	−24.771
O	0.9237	0.8710	−20.703	−25.647

We have analyzed Ce L_3 XANES by calculating the expected absorption spectrum for one-electron transitions from the $2p$ core level to the Ce $5d$ unoccupied states of a large cluster of atoms including final-state effects. By using our approach, the crystal-field splitting of Ce $5d$ states can be predicted and compared with experimental data.

A first step in the multiple-scattering analysis of XANES data is the determination of the minimum size of the cluster of neighbor atoms around the absorbing Ce atom, within which the scattering of the photoelectron can reproduce the entire fine structure of XANES. In Fig. 1 we report the results of a Ce L_3 XANES calcula-

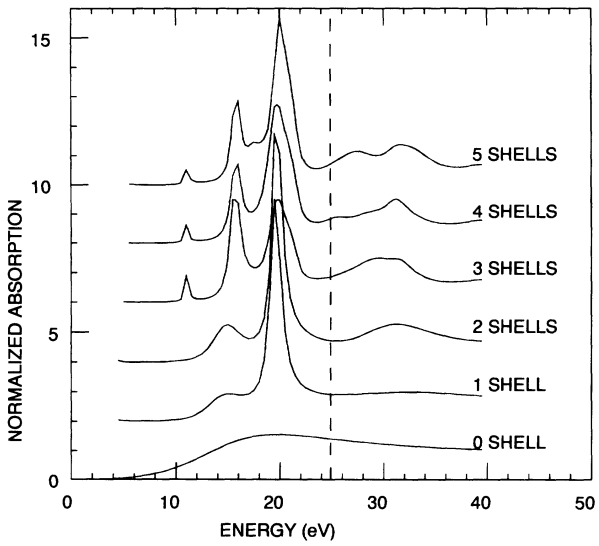

FIG. 1. Normalized x-ray-absorption coefficient for the Ce L_3 edge of CeO_2 calculated in the fully relaxed final-state potential within clusters of different sizes. Contributions from the two $\Delta l = \pm 1$ channels are included. Each spectrum is shifted along the y axis by a value of 2.0 relative to the previous value. The absorption coefficient has been normalized to the value of the atomic absorption at high energies α_0. The zero of the energy scale is chosen at the average fully relaxed interstitial potential (i.e., the muffin-tin zero) V_0 of the Ce atom. The vertical dashed line marks the vacuum level position.

tion for CeO_2 in the fully relaxed potential by considering clusters of different size (the zero-shell cluster corresponds to the atomic absorption). The spectrum is the sum of the two $\Delta l = \pm 1$ dipole-allowed channels. All spectra have been normalized to the value of the absorption coefficient at high energy (above 40 eV) and shifted along the y axis by the value of 2.0. The peak at about 11 eV above the energy of the muffin-tin zero appears only when three or more shells are included in the cluster calculation. The peak at the energy of 16 eV becomes a well-pronounced feature with an intensity relative to the main white line peak and the energy separation between them in agreement with the experimental spectrum only for the four- and five-shell clusters. Therefore we conclude that these low-energy peaks are a result of multiple scattering of the excited photoelectron within a cluster of large size (not less than about 45 atoms), showing that the final state reached in the core transitions (the white lines) is not a simple atomic or molecular state. We must stress that it is only on the basis of a multiple-scattering calculation within a cluster of large size that we succeed in obtaining the presence of additional low-energy features at 11 and 16 eV. These low-energy shoulders were not obtained numerically in previous calculations. There have been only a few attempts to interpret them qualitatively as shakedown satellites,[8] or as due to a quadrupole (prepeak at 11 eV) or to a depopulation of mixed Ce $5d$–O $2p$ states during the relaxation process.[3]

In order to understand the origin of the experimental features in Ce L_3 XANES spectra, it is important to calculate the electronic transitions from different atoms and at unoccupied states with different symmetries. XANES calculations in the initial-state potential using a five-shell cluster are reported in Fig. 2. The normalized absorption

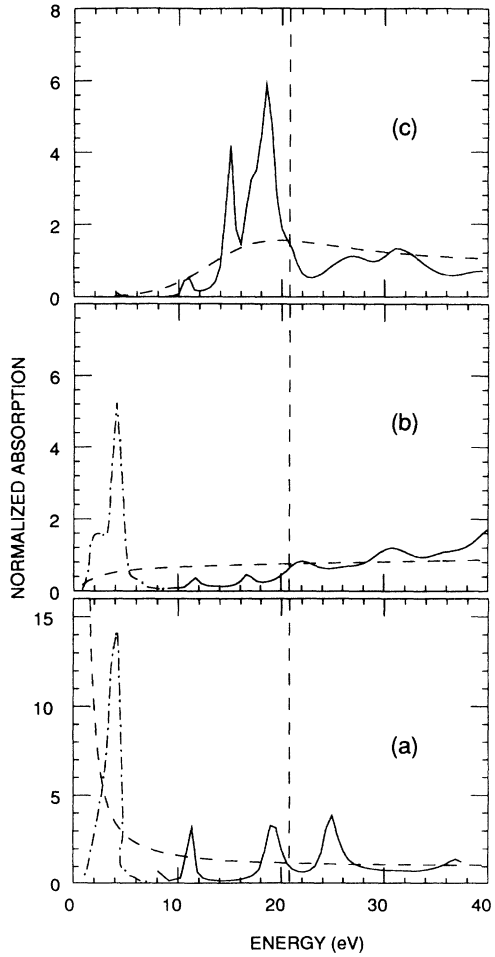

FIG. 2. Calculated cross sections for O $1s \rightarrow \varepsilon p$ (a), Ce $1s \rightarrow \varepsilon p$ (b), and Ce $2p \rightarrow \varepsilon d$ (c) transitions for the large-size cluster (five shells) in the ground-state potential of CeO_2. The zero of the energy scale is chosen at the average interstitial potential V_0 of the central Ce atom for the ground-state potential. The solid line shows the unoccupied states, the dash-dotted line the occupied states. Atomic cross sections (i.e., for zero-shell cluster) are shown by dashed curves.

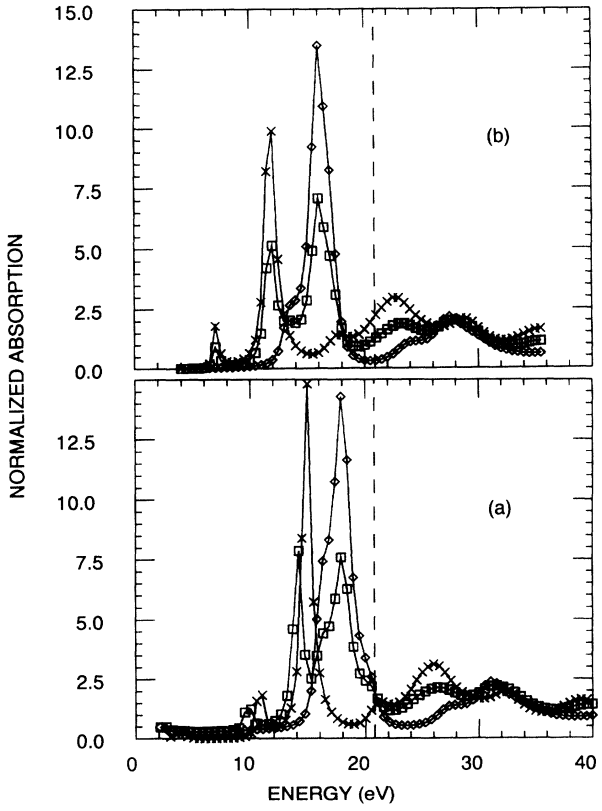

FIG. 3. (a) Calculated partial cross sections for dipole transitions from the Ce $2p$ core level to $5d$ states, with angular momentum $m_l = 0$ (crosses), $m_l = 1$ (diamonds), and $m_l = 2$ (squares) in the initial-state (unrelaxed) potential for a cluster of five shells. (b) Calculated partial cross sections for the Ce $2p \rightarrow \varepsilon d$ transitions to final states with angular momentum $m_l = 0$ (crosses), $m_l = 1$ (diamonds), and $m_l = 2$ (squares) for a cluster of five shells in the fully relaxed potential. The zero of the energy scale is chosen at the average interstitial potential V_0 for the central Ce atom in the unrelaxed potential.

coefficient data correspond to the Ce-projected partial $5d$ density of states [see Fig. 2(c)] times the matrix element. To complete the information about the distribution of unoccupied electronic states in the CeO_2 crystal, we also calculated the partial cross sections for Ce states of p symmetry [Fig. 2(b)] as well as oxygen p symmetry [Fig. 2(a)]. These data have to be compared with results of band-structure calculations.[2,3] The advantage of our results compared with previous ones is that we have analyzed partial densities of unoccupied states separately.

The joint analysis of these curves shows a very interesting effect of the mutual influence of p and d symmetry states in the conduction band of CeO_2. The electronic states with p symmetry are pushed out of the energy interval from 12 to 15 eV, where Ce $5d$ states are localized. Previously such interaction was observed only between p and d states in the valence band[32] and for ligand p rare-earth f states in the conduction band of NdS.[33] This kind of resonance interaction can be shown to be of great importance in a large number of compounds.[34]

The method we used permits us to obtain partial cross sections, corresponding to transitions of electrons with different projections of angular momentum ($m_l=0$, 1, and 2). In Fig. 3(a) we report the partial cross sections, calculated in the ground-state potential of CeO_2. Ce $5d$ states are split in the cubic crystal field of eight oxygen atoms into two degenerate low-energy e_g levels: $5d_{3z^2-r^2}$ (with $m_l=0$ orbital angular momentum) and $5d_{xy}$ (with $m_l=2$ orbital angular momentum); and three degenerate high-energy t_{2g} levels: $5d_{xz}$, $5d_{yz}$ (i.e., two states with $m_l=1$ orbital angular momentum) and $5d_{x^2-y^2}$ (with $m_l=2$ orbital angular momentum).

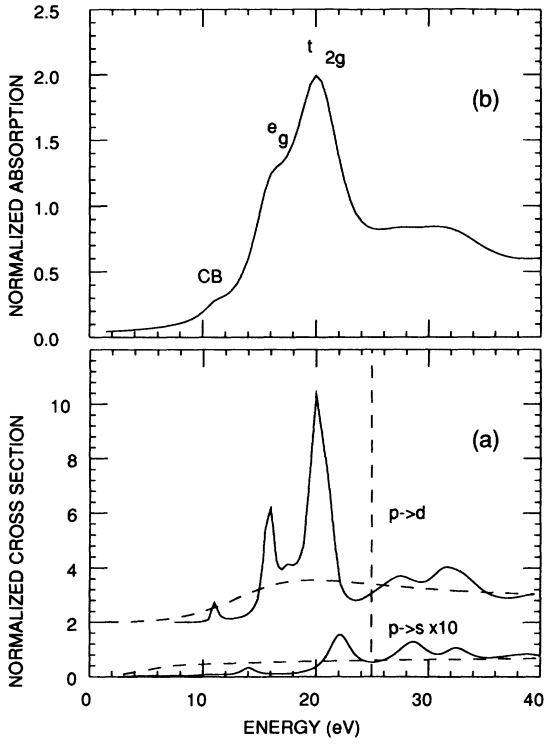

FIG. 4. (a) Calculated normalized cross sections for dipole $\Delta l=\pm 1$ transitions from the Ce $2p$ core level to εd states and to εs states in the final-state (relaxed) potential for a cluster of five shells. (b) Calculated Ce L_3-edge XANES in CeO_2 within a cluster of five shells in the fully relaxed potential, taking into account all the broadening factors, including the two $\Delta l=\pm 1$ channels.

It is well known that final states in the x-ray-absorption process are perturbed by the core hole–photoelectron interaction, especially in the case of $L_{2,3}$-edge XANES.[25,26] In Fig. 3(b) we present the same partial cross sections as in Fig. 3(a), but calculated in the fully relaxed potential of the final state, including the core hole relaxation effect. In the case of Ce L_3 XANES the core hole–photoelectron interaction results in a relative energy shift of the absorption peaks. Therefore in order to compare present calculations with experimental data we performed multiple-scattering calculations in the fully relaxed potential using the $Z+1$ approximation.

An important fact that can be extracted by comparison of Figs. 3(a) and 3(b) is that the line shape and energy splitting of the white lines in the initial- and final-state potentials are different. The crystal-field splitting measured as the splitting between the two lines is $\Delta_i=3.5$ eV in the initial state and $\Delta_f=4.0$ eV in the final fully relaxed state. The final-state energy splitting Δ_f can be described as the crystal-field splitting of the Pr $5d$ levels of a Pr impurity (at the Ce site) in the crystal; therefore it must be different from Δ_i.

According to dipole selection rules the electronic transition corresponding to Ce L_3 XANES includes two $\Delta l=\pm 1$ channels: $2p\rightarrow\varepsilon d$ and $2p\rightarrow\varepsilon s$. In Fig. 4(a) we report calculations of the partial cross sections, corresponding to these two transitions in the fully relaxed final-state potential. Because of a small relative value of the transition matrix element for the $2p\rightarrow\varepsilon s$ channel in the near-edge energy region, the contribution of the $2p\rightarrow\varepsilon s$ partial cross section to the total Ce L_3 XANES spectrum of CeO_2 was found to be negligible.

In order to perform a direct comparison with experimental data, one must take into account two factors: (1) the filling of occupied states following the Fermi distribution; and (2) the broadening of experimental spectra due to the core hole lifetime, the finite mean free path of the photoelectron, and experimental resolution. The resulting broadening factor has been treated as contributing the imaginary part of the complex muffin-tin potential. We have used for the L_3 core hole bandwidth the value of 2.5 eV;[35] for the mean free path of the electron, we have taken the energy-dependent function obtained in Ref. 36, and for the experimental energy resolution we used the value of 1.0 eV. In Fig. 4(b) we present Ce L_3 XANES in CeO_2 calculated within a cluster of five shells in the fully relaxed potential, and taking into account the convolution of these broadening factors, including the two $\Delta l=\pm 1$ channels.

III. MANY-BODY TREATMENT

The electronic structure of the correlated CeO_2 system, where there is a large mixing between localized $4f$ levels

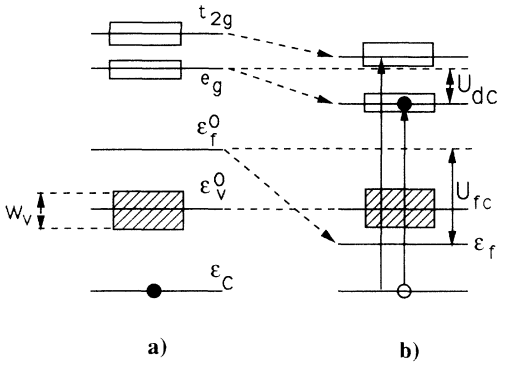

FIG. 5. Pictorial scheme for the initial (a) and final (b) states in CeO_2.

and more delocalized O $2p$ levels, can be described by mixing of the multielectron configurations: $4f^0$ and $4f^1\underline{L}$, where L denotes a ligand (O $2p$) hole. These two configurations before hybridization are separated by the charge-transfer energy Δ. The hybridization energy V between the atomiclike localized $4f$ and delocalized O $2p$ states determines the mixing between the multielectron configurations. The electronic Coulomb repulsion U_{ff} describes the correlation of localized f states. The final state of Ce L_3 XANES is determined by the Coulomb interactions U_{dc} between the $5d$ electron and the core hole, and U_{fc} between the f electrons and the core hole, and the Coulomb repulsion U_{df} between the $5d$ and f electrons. As was shown[9] within this formalism, one can reproduce the two main peaks of experimental Ce L_3 XANES in CeO_2 [A and B in our notation in Fig. 5(c)], but the low-energy features (C and D) were not obtained.

The full multiple-scattering predictions of the final states of CeO_2 (Sec. II) show that the crystal-field splitting of Ce $5d$ states is larger than the width of $5d$ final states and the experimental resolution. One needs to take this effect into account in the analysis of L_3 XANES. We have also succeeded in estimating crystal-field splitting for both initial and final states of Ce L_3 absorption. Having this information, we can expand the many-body approach,[9] introducing the Ce $5d$ state crystal-field splitting. The general scheme of the present calculation was the same as in Ref. 9, therefore here we present only the set of parameters we have used. In Fig. 5 we show our model for Ce L_3 XANES in CeO_2, both in the initial [Fig. 5(a)] and final [Fig. 5(b)] states.

Two Ce $5d$ bands split by the crystal field $f=4$ eV are simulated by two sets of discrete levels: one for e_g and another for t_{2g} orbitals, with the ratio of the band density of states 2:3. The energy separation between the $4f$ level ε_f^0 and the center of the O $2p$ valence band is assumed to be 1.6 eV. The value of $U_{ff}=10.5$ eV (in agreement with findings from XPS core spectra[19]) has been assumed to describe the ground state. The value of $U_{fc}=12.5$ eV was determined from Ce ($3d$) XPS spectra as represented in Ref. 19. $U_{dc}=4$ eV and $U_{df}=3$ eV were used. The oxygen $2p$ bandwidth W_v in CeO_2 was taken to be 3 eV [see Fig. 2(a)], in agreement with band-structure calcula-

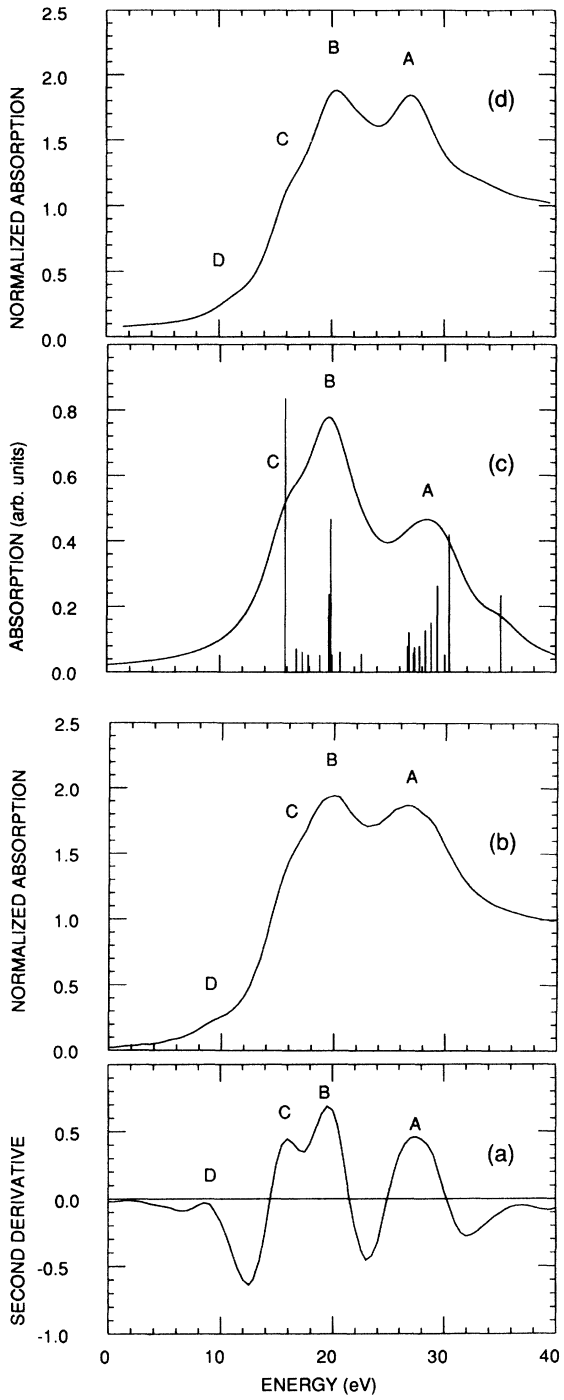

FIG. 6. (a) Second derivative of the experimental Ce L_3 XANES in CeO_2. (b) Experimental Ce L_3 XANES in CeO_2 from Ref. 9. (c) Calculated spectrum of many-body final states in the frame of the Anderson impurity model, including the crystal-field splitting of the $5d$ final states. (d) Approximate simulation of the convolution of the two main photoabsorption channels in the potentials of two many-body configurations of the relaxed $N-1$ passive electrons $4f^1L$ and $4f^0$, (neglecting $4f^2L^2$) obtained by summing two one-electron spectra (including the two $\Delta l=\pm 1$ channels), obtained by multiple-scattering calculations [Fig. 4(b)] with relative weights 0.66 and 0.33, respectively, and energy separation of 7 eV. The theoretical spectra in (c) and (d) have been aligned to the energy position of the experimental peak B.

tions.[2,3] To take this effect into account, we treat the valence band as a finite system consisting of six discrete levels, being situated within an energy interval of 3 eV around the center of the band. The spectral broadening due to the finite lifetime of the core hole was introduced by an additional broadening term equal to 2.5 eV. In this many-body treatment we neglect the contribution of the $p \rightarrow s$ channel.

In Fig. 6 we show experimental Ce L_3 XANES in CeO_2 from Ref. 9 [Fig. 6(b)] and its second derivative [Fig. 6(a)]. The result of the many-body calculations is presented in Fig. 6(c). As far as one can see, the development of the previous model,[9] by the introduction of the crystal-field effect, results in a good agreement between theoretical and experimental spectra and supports the interpretation of the low-energy shoulder C in Ce L_3 XANES of CeO_2 as being due to the crystal-field splitting of Ce $5d$ states.

The pre-edge structure, labeled D, is not reproduced by the many-body calculation. The reason is that here we have not fully introduced the band character of Ce d unoccupied states in CeO_2, and, particularly, the maximum of d states at the bottom of the conduction band [labeled CB in Fig. 4(b)], which appears to be a result of multiple scattering of the photoelectron within large size clusters (at least 45 atoms), including two shells of oxygen atoms. This feature is therefore assigned to final states with delocalized d character at the bottom of the conduction band.

In order to reproduce the full experimental spectrum, we can describe, in a first approximation, the CeO_2 spectrum as arising from the convolution of two channels corresponding to transitions $2p \rightarrow \varepsilon d$ in the two relaxed potentials of the two main many-body configurations of the $N-1$ passive electrons $4f^0$ and $4f^1\underline{L}$ (neglecting $4f^2\underline{L}^2$). Therefore in Fig. 6(d) we have plotted the convolution of two calculated spectra for one-electron transitions separated by 7 eV, and with a relative statistical weight from 0.66 to 0.33. As one can see in Fig. 6(d), the agreement of the model's theoretical spectrum with the experimental one is good enough. It is clear that the quantitative prediction of the Ce L_3 XANES spectrum requires one to introduce the fine structure of the full partial density of d states in the CeO_2 conduction band into the Anderson impurity model.

In conclusion, a combined study of the Ce L_3 x-ray-absorption near-edge structure of CeO_2 based on both multiple-scattering analysis and many-body treatment in the framework of the Anderson impurity model, including the crystal-field splitting effect, has been carried out. We have shown that the crystal structure effects influence Ce L_3 absorption near-edge structure in CeO_2. The wave function of the excited electron in the final states of the Ce L_3-edge XANES spectrum is found to be determined by multiple-scattering processes in a large size cluster formed by at least 45 atoms. The partial distributions of Ce-projected unoccupied states in the ground state with p and d (t_{2g} and e_g) symmetries and O p symmetry in the conduction band of CeO_2, have been calculated. The crystal-field energy splitting in the initial state Δ_i is found to be about 3.5 eV. Agreement between calculated ($\Delta_f = 4.0 \pm 0.2$ eV) and experimental ($\Delta_f = 3.7 \pm 0.5 eV$) crystal-field energy splittings for Ce $5d$ final states in L_3 spectra is found. It was shown that crystal-field splitting of Ce $5d$ states plays the key role in the formation of a low-energy shoulder in Ce L_3-edge XANES of CeO_2. A low-energy prepeak in Ce L_3-edge XANES of CeO_2 has been found to be due to the multiple scattering of the photoelectron within a cluster of large size (45 atoms), including at least two shells of oxygen atoms.

ACKNOWLEDGMENTS

This research was partially supported by NATO Grant No. CRG 930305 and a grant from the Russian Ministry of Science and Education. This work was partially carried out in the framework of the exchange program between the Japan Society for Promotion of Science and National Research Council of Italy. One of us (A.B.) would like to thank the Institute of Solid State Physics in Tokyo for kind hospitality. One of us (A.V.S.) would like to acknowledge the kind hospitality of Rome University and Dr. A. Marcelli for discussions.

[1] J. L. Smith and P. S. Riseborough, J. Magn. Magn. Mater. **47&48**, 545 (1985).

[2] D. D. Koelling, A. M. Boering, and J. H. Wood, Solid State Commun. **47**, 227 (1983).

[3] L. D. Finkelstein, A. Postnikov, N. N. Efremova, and E. Z. Kurmaev, Mater. Lett. **14**, 115 (1992).

[4] G. Thornton and M. J. Dempsey, Chem. Phys. Lett. **77**, 409 (1981).

[5] E. E. Vainsthein, S. M. Blokhin, and Yu. B. Paderno, Fiz. Tverd. Tela (Leningrad) **6**, 2909 (1965) [Sov. Phys. Solid State **6**, 2318 (1965)].

[6] R. C. Karnatak, J. M. Esteva, H. Dexpert, M. Gasgnier, P. E. Caro, and L. Albert, J. Magn. Magn. Mater. **63&64**, 518 (1987).

[7] A. Bianconi, I. Davoli, S. Della Longa, J. Garcia, K. B. Garg, A. Kotani, and A. Marcelli, in *Theoretical and Experimental Aspects of Valence Fluctuations and Heavy Fermions*, edited by L. C. Gupta and S. K. Malik (Plenum, New York, 1987), p. 243.

[8] H. Dexpert, R. C. Karnatak, J. M. Esteva, J. P. Coonerade, M. Gasgnier, P. E. Caro, and L. Albert, Phys. Rev. B **36**, 1750 (1987).

[9] A. Bianconi, A. Marcelli, H. Dexpert, R. Karnatak, A. Kotani, T. Jo, and J. Petiau, Phys. Rev. B **35**, 806 (1987).

[10] P. Burroughs, A. Hamnett, A. F. Orchard, and G. Thornton, J. Chem. Soc. Dalton Trans. **17**, 1686 (1976).

[11] G. Krill, J. P. Kappler, A. Meyer, L. Abadli, and M. Ravet, J. Phys. F **11**, 1713 (1981).

[12]K. R. Bauchspiess, W. Boksch, E. Holland-Moritz, H. Launois, R. Pott, and D. H. Wohlleben, in *Valence Fluctuations in Solids,* edited by L. M. Falicov, W. Hanken, and M. B. Maple (North-Holland, Amsterdam, 1981), p. 417.

[13]A. Bianconi, M. Campagna, and S. Stizza, Phys. Rev. B **25**, 2477 (1982).

[14]A. Bianconi, A. Marcelli, M. Tomellini, and I. Davoli, J. Magn. Magn. Mater. **47&48**, 209 (1985).

[15]J. Bloch, N. Shamir, M. H. Mintz, and U. Atzmony, Phys. Rev. B **30**, 2462 (1984).

[16]E. Wuilloud, B. Delley, W.-D. Schneider, and Y. Baer, Phys. Rev. Lett. **53**, 202 (1984).

[17]A. Kotani and Y. Toyozawa, J. Phys. Soc. Jpn. **35**, 1073 (1973); **35**, 1082 (1973); **37**, 912 (1974).

[18]T. Jo and A. Kotani, Solid State Commun. **54**, 451 (1985).

[19]A. Kotani, H. Mizuta, T. Jo, and J. C. Parlebas, Solid State Commun. **53**, 805 (1985).

[20]A. Kotani and J. C. Parlebas, J. Phys. (Paris) **46**, 77 (1985).

[21]H. L. Schläfer and G. Gliemann, *Basic Principles of Ligand Field Theory* (Wiley-Interscience, London, 1969).

[22]A. Bianconi, in *X Ray Absorption: Principles, Applications and Techniques of EXAFS, SEXAFS and XANES,* edited by R. Prinz and D. Koningsberger (Wiley, New York, 1988), p. 537.

[23]P. Kizler, Phys. Lett. A **172**, 66 (1992).

[24]R. V. Vedrinskii, L. A. Bugaev, I. I. Gegusin, V. L. Kraizman, A. A. Novakovich, S. A. Prosandeev, R. E. Ruus, A. A. Maiste, and M. A. Elango, Solid State Commun. **44**, 1401 (1982).

[25]A. Borg, P. L. King, P. Pianeta, I. Lindau, D. B. Mitzi, A. Kapitulnik, A. V. Soldatov, S. Della Longa, and A. Bianconi, Phys. Rev. B **46**, 8487 (1992).

[26]A. V. Soldatov, S. Della Longa, and A. Bianconi, Solid State Commun. **85**, 863 (1993).

[27]J. Guo, D. E. Ellis, G. L. Goodman, E. E. Alp, L. Soderholm, and G. K. Shenoy, Phys. Rev. B **41**, 82 (1990).

[28]Z. Y. Wu, M. Benfatto, and C. R. Natoli, Phys. Rev. B **45**, 531 (1992).

[29]D. D. Vvedensky, D. K. Saldin, and J. B. Pendry, Comput. Phys. Commun. **40**, 421 (1986).

[30]R. W. G. Wyckoff, *Crystal Structure* (Interscience, New York, 1963).

[31]C. Li, M. Pompa, A. Congiu-Castellano, S. Della Longa, and A. Bianconi, Physica C **175**, 369 (1990).

[32]E. P. Domashevskaya and V. A. Terekhov, Phys. Status Solidi B **121**, 121 (1981).

[33]A. V. Soldatov and A. N. Gusatinskii, Phys. Status Solidi B **125**, 129 (1984).

[34]A. A. Lavrentiev, A. N. Gusatinskii, M. A. Blokhin, A. V. Soldatov, V. A. Letnev, and I. V. Bodnar, J. Phys. C **20**, 3445 (1987).

[35]O. Keski-Rahkonen and M. O. Krause, At. Data Nucl. Data Tables **14**, 139 (1974).

[36]J. E. Muller, O. Jepsen, and J. W. Wilkins, Solid State Commun. **42**, 365 (1982).